## 1.5 The Effect of Bulk Oxygen Concentration on the Micro-nanostructure and Strength of a 14Cr Nanostructured Ferritic Alloy

— Y. Wu, N. J. Cunningham, A. Etienne,[1] E. Haney, G. R. Odette (University of California Santa Barbara), E. Stergar (Leoben University),[2] D. T. Hoelzer (Oak Ridge National Laboratory), B. D. Wirth (University of California Berkeley[3]) and S. A. Maloy (Los Alamos National Laboratory)

### OBJECTIVE

The objective is to evaluate the effect of bulk O on the microstructure, nanofeatures and hardness of nanostructured ferritic alloys (NFA) that otherwise have a generally similar compositions and processing paths.

### SUMMARY

The effects of bulk O variations on the characteristics of the grain structure, nanofeatures (NFs) and microhardness of nanostructured ferritic alloys (NFA) were investigated. The grain structures were characterized by optical metallography and transmission electron microscopy (TEM). The NFs were characterized by TEM, atom probe tomography (APT) and small angle neutron scattering (SANS). Based on bulk chemical analysis of the milled powders, the O content ranged from 0.065 to 0.249 (wt.%). The variations in O resulted from differences in the milling conditions. The low O powders (OW3) were milled with a procedure that minimized contamination, while the high O powders (OW1), that initially had a low O content in the as atomized condition, were contaminated with both N and O during milling. The intermediate O powders (OW4) minimized this contamination while increasing O with additions of FeO during milling. The three powder batches were all consolidated by hot isostatic pressing (HIPing) at 1150°C and 200 MPa. All the consolidated alloys had bimodal distributions of grain sizes, that were characterized by the two average large and small sizes ($d_{s,l}$) and the relative fraction of the small grains ($f_s$). The NFs were Y-Ti-O enriched phases characterized by their number density (N), size distributions and average diameter (<d>), composition (especially the Y/Ti ratio) and phase structure (not evaluated in this study). Both the large and small grain sizes decreased with increasing O contents, while the fraction of small grains increased. The size of the NFs decreased and their number density increased with increasing O. TEM energy dispersive x-ray (EDX) studies indicated the low O alloy contained fewer and coarser features compared to alloys with higher O. TEM showed that the low O features were much more highly enriched in Y compared to Ti, including a majority that contained no Ti. However, APT showed that NFs in the low O alloy with <d> ≈ 5 nm had Y/Ti ratios < 1 that is only slightly larger than found in the other cases. The Vickers microhardness ($H_v$) of the alloys increased significantly with increasing O, reflecting both the effects of differences in the grain size and scale dispersion strengthening features. The $H_v$ increased systematically with the volume fraction of NFs measured by SANS.

---

[1] Current institution Rouen University
[2] Current institution University of California Santa Barbara and Berkeley
[3] Current institution University of Tennessee Knoxville

## PROGRESS AND STATUS

Ohtsuka, Ukai and their co-workers have shown that the O content of 9 Cr steels, that are transformable analogs to NFAs, has a strong effect on both their micro-nanostructures and properties [1-3]. This is in part attributed to an O effect on the composition and scale of the dispersion strengthening oxides and in part due to the effect of O on the fraction of ferrite versus martensite in the normalized and tempered alloys. Decreasing O was reported to lead to oxides richer in Y and to a decrease in the fraction of the ferrite phase where the NFs preferentially form.

This work is part of a collaborative program to develop a larger best practice heat of 14Cr NFA [4]. The alloys in this study were fabricated from atomized Fe-14Cr-0.4Ti-0.2Y powders. The addition of Y was intended to explore the possibility of minimizing, or eliminating, the milling step normally used to mix $Y_2O_3$ into solid solution. However, it was found that the Y phase separates during atomization and that extensive milling is still needed prior to consolidation, in this case by HIPing at 1150°C and 200 MPa. The main focus of this work has been on the powders with low O. The first milling procedure that was used added O and N to the powders as a contaminant (OW1). An improved milling procedure reduced the contamination (OW3). However, as described below, the low O in this alloy resulted in low hardness and coarser grain and NF structures. Thus more O was added to the initially low O powders by milling them with FeO (OW4). Examining the micro-nanostructure and hardness of the three alloys provides an opportunity to assess the effects of O in a non-transformable fully ferritic 14Cr alloy.

## EXPERIMENTAL PROCEDURES

The experimental procedures are only very briefly outlined here. Full details will be provided in future reports and publications. The as atomized alloy powders described above were provided by ATI Powder Metals, along with their bulk chemical compositions. Milling was carried out for 40h in a dry Ar atmosphere using a Zoz Simolayer CM-01 attritor mill at UC Berkeley (OW1 and 3) and in a CM-08 attritor mill at Oak Ridge National Laboratory (OW4). The grain structures were characterized by optical metallography and TEM. The NFs were characterized by TEM, APT and SANS. The Vickers microhardness of the alloys was measured at a 500 g load. The compositions of the powders used in this study are shown in Table 1. OW1 and OW4 alloys used the -100/+325 mesh L2311 powder, while OW3 used the -325 mesh L2314 powder. Table 2 shows the O and N contents of the three powders after milling.

**Table 1. ATI powder compositions (wt%).**

| Batch | Mesh | Alloy | Fe | Cr | W | Ti | Y | Al+Si | O | N | C |
|---|---|---|---|---|---|---|---|---|---|---|---|
| L2311 | -100/+325 | OW1, 4 | Bal | 14.0 | 3.0 | 0.35 | 0.21 | 0.045 | 0.014 | 0.002 | 0.006 |
| L2314 | -325 | OW3 | Bal | 14.0 | 3.0 | 0.36 | 0.21 | 0.045 | 0.034 | 0.002 | 0.005 |

**Table 2: N and O wt% in the milled powders used for OW1, OW3 and OW4 HIP alloys (wt.%).**

| Alloy | N | O |
|---|---|---|
| OW1 | 0.190 | 0.249 |
| OW3 | 0.016 | 0.065 |
| OW4 | 0.013 | 0.127 |

## RESULTS

As shown in Figure 1, all the NFA had bimodal grain structure with large grains up to tens of μm or, and small grains d < 1 μm. Table 3 summarizes the grain structures, characterized by the two average large and small sizes ($d_{s,l}$) and relative fraction of the small grains ($f_s$). The $d_l$ increase and the $f_s$ decrease systematically with decreasing O. The highest O OW1 alloy has the smallest $d_l$. However, systematic ordering of $d_s$ is not observed in the intermediate and low O alloys.

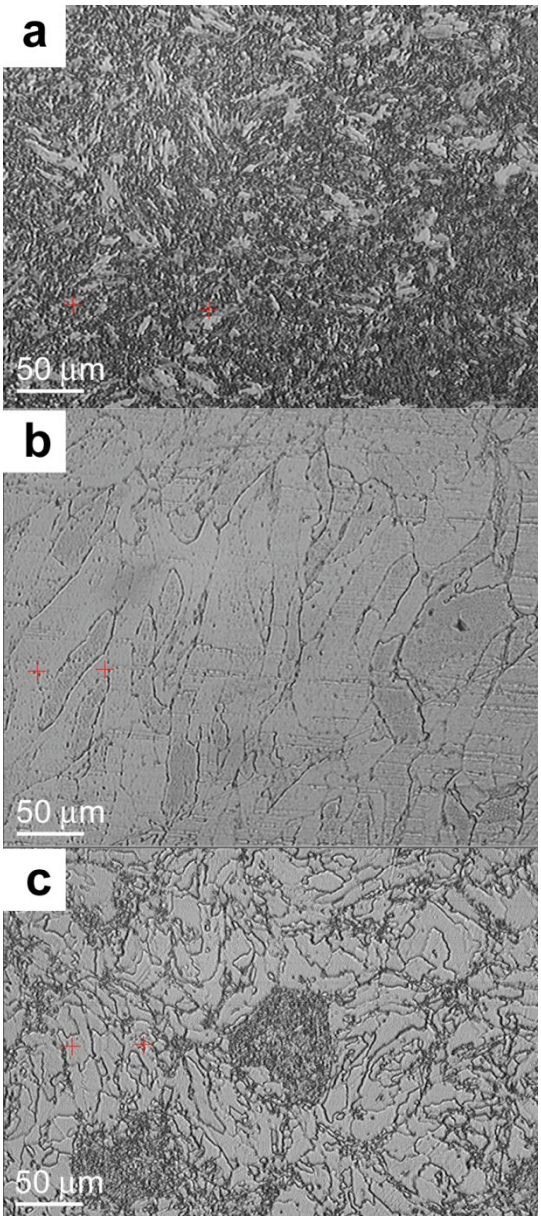


**Figure 1. Optical micrographs of etched (a) OW1, (b) OW3, and (c) OW4.**

**Table 3. The average large and small grain sizes ($d_{s,l}$) and relative fraction of the small grains ($f_s$) in OW1, OW3 and OW4.**

| Alloy | $d_l$ (µm) | $d_s$ (nm) | $f_s$ (%) |
|---|---|---|---|
| OW1 | 9.4 | 151 | 70 |
| OW3 | 23.3 | 323 | 2 |
| OW4 | 11.3 | 582 | 10 |

TEM micrographs showing the NFs in OW1, OW3 and OW4 are shown in Figure 2. Figure 3 compares the corresponding size distributions. The size and concentration of the NFs in low O, OW3 are <d> ≈ 4.7 nm and N ≈ $6.2\times10^{22}/m^3$, respectively, while those in intermediate O, OW4 are <d> ≈ 2.4 nm and $2.8\times10^{23}/m^3$. The NFs in high O, OW 1 are only slightly coarser compared to those in OW4 with <d> ≈ 3.4 nm and N ≈ $1.2\times10^{23}/m^3$.

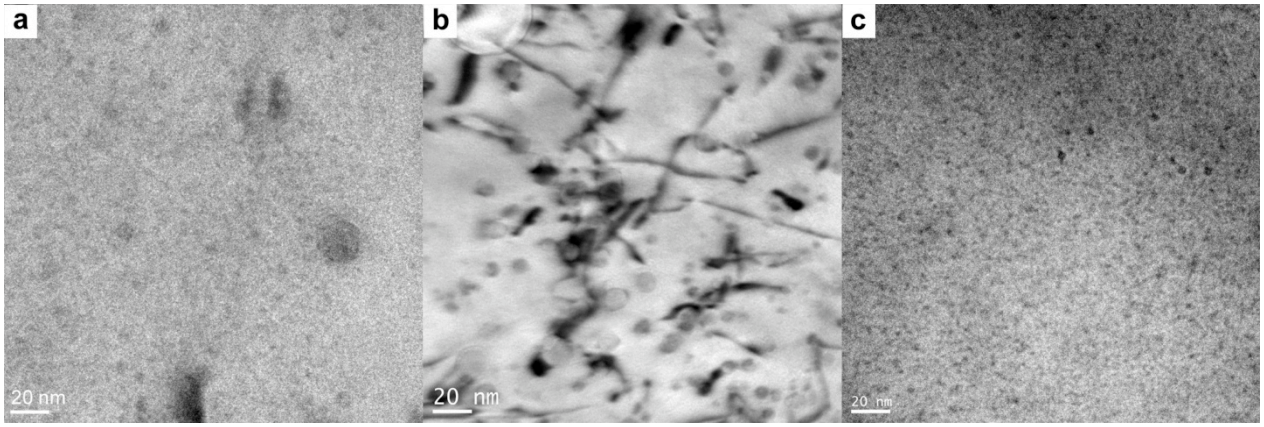


**Figure 2. TEM micrographs of the NFs in OW1 (a), OW3 (b) and OW4 (c).**

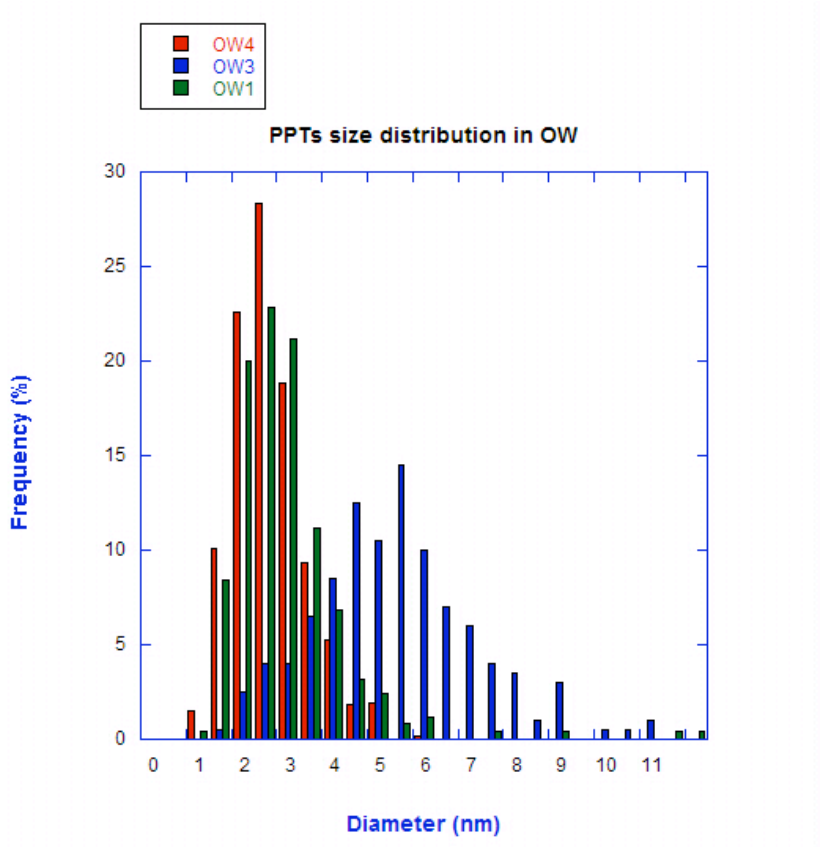


**Figure 3. The size distributions of the NFs in OW1, OW3 and OW4 measured by bright field TEM.**

EDX was also used to estimate the compositions of NFs extracted on C foils. Figure 4 shows EDX measurements on individual precipitates in OW3, while Figure 5 shows the EDX spectrum for a broad area containing many smaller NFs in OW4. In the low O, OW3 alloy, 15 out of the 20 precipitates observed were Y-rich and contained no Ti (average diameter ≈ 7.0 nm), while 1 had a Y/Ti ratio between 1 and 2 (diameter ≈12.0 nm) and 4 had ratios between 2 and 10 averaging 4.6 (average diameter ≈ 6.0 nm). In contrast the average Y/Ti ratio in the medium O, OW4, was 0.5 and 1.2 (d<5 nm), 2.3 (5<d<10 nm) in the high O, OW1.

**Table 3. The NF N and <d> measured by TEM.**

| Alloy | <d> (nm) | N ($10^{23}/m^3$) |
|---|---|---|
| OW1 | 3.4 | 1.2 |
| OW3 | 4.7 | 0.6 |
| OW4 | 2.4 | 2.8 |

Figure 6 shows examples NFs found in the APT studies of OW1, OW3 and OW4. The corresponding N and <d> are summarized in Table 4. In OW3 <d> = 5.8 nm and N = $6.0\times10^{22}/m^3$. This is in contrast to the smaller diameters of 1.7 nm and 2.5 nm and higher number densities of $2.9\times10^{23}/m^3$ and $9.6\times10^{23}/m^3$ for OW1 and OW4, respectively. The Y/Ti/O ratios for OW1, OW3, and OW4 were 23/37/41, 22/31/46, and 11/42/47 respectively. OW3 has the highest Y/Ti ratio, but it is still less than 1.

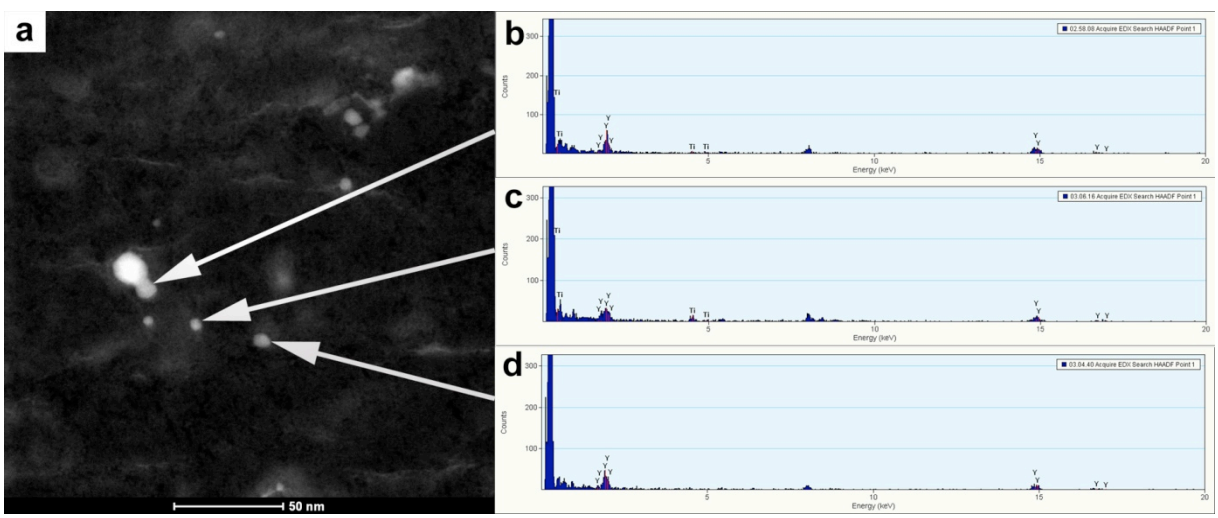


**Figure 4. STEM image of an extraction replica sample from OW3 (a); EDX spectra from the PPTs marked by the arrows (b)-(d).**

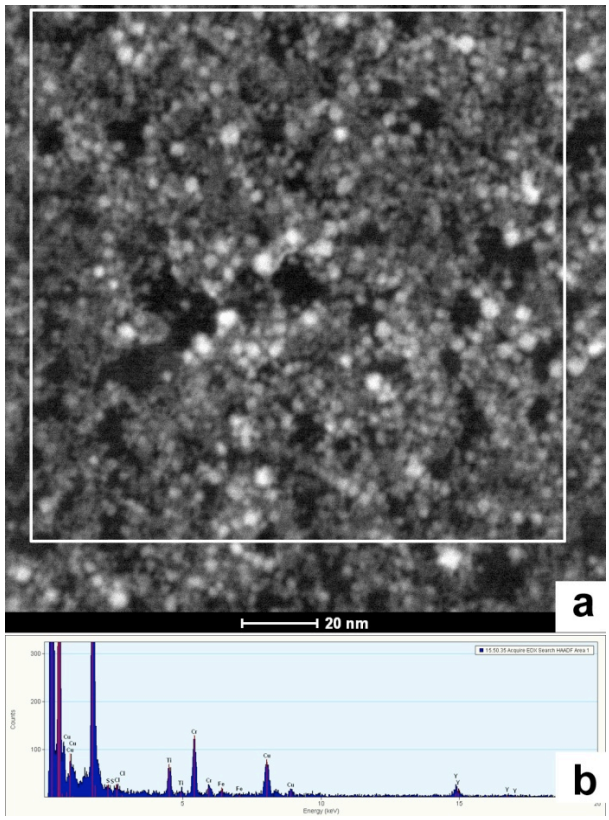


**Figure 5. STEM image of an extraction replica sample from OW4 (a); EDX spectrum of the square area in (a) is shown in (b).**

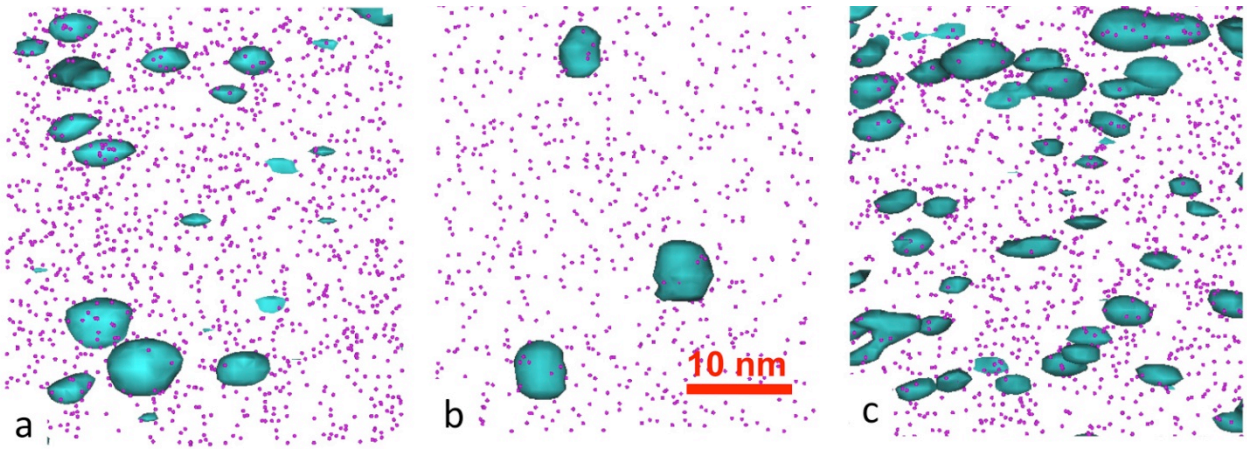


**Figure 6. 20 nm thick Atom maps with Cr ions and Y-Ti-O isoconcentration surfaces (4.0%) for (a) OW1, (b) OW3, and (c) OW4.**

**Table 4. The NF number density (N) and average diameter (<d>) measured by APT.**

| Alloy | <d> (nm) | N ($10^{23}/m^3$) |
|---|---|---|
| OW1 | 1.7 | 2.9 |
| OW3 | 5.8 | 0.7 |
| OW4 | 2.5 | 9.6 |

SANS was performed on OW1, OW3, and on an L2314 powder attritor milled with FeO and annealed for 3 h at 1150ºC, which is expected to be representative of OW4. OW1 and the OW4 surrogate FeO milled and annealed powder had smaller <d> = 2.8 nm, while low O, OW3 had larger <d> = 5.4 nm. High O, OW1 had N = $1.1\times10^{24}/m^3$, while the intermediate O, OW4 surrogate FeO milled and annealed powder had N = $7.1\times10^{23}/m^3$. Consistent with the TEM and APT results, the low O, OW3 had the lowest N =$5.2\times10^{22}/m^3$. The nominal NF volume fractions for the OW1, OW3 and OW4 surrogate and OW3 were 1.2, 0.8 and 0.4% respectively.

**Table 5. The NF N and <d> measured by SANS.**

| Alloy | <d> (nm) | N ($10^{23}/m^3$) | f |
|---|---|---|---|
| OW1 | 2.8 | 11 | 1.2 |
| OW3 | 5.4 | 0.5 | 0.4 |
| OW4* | 2.8 | 7.1 | 0.8 |

*Powder milled with FeO and annealed.

## DISCUSSION

A summary of the NF sizes and number densities for the three techniques is shown in Table 6, along with the APT Y/Ti/O ratios and microhardness values. Figure 7 shows the average N and <d> for the three techniques as a function of the alloy O content. The NF characteristics are similar at the intermediate and high O levels, but as noted previously, the NF are larger and much fewer in number in case of the lowest O. Figure 8 shows that the microhardness increases with O. Table 6 also shows the microhardness ($H_v$) and the NF volume fraction (f) measured by SANS. Notably, as shown in Figure 9, $H_v$ increases in direct proportion to the $\sqrt{f}$.

**Table 6. Summary of the N and <d> in OW1, OW3 and OW4 measured by TEM, APT and SANS.**

| Technique | OW1 | OW3 | OW4 |
|---|---|---|---|
| O (wt.%) | 0.249 | 0.065 | 0.127 |
| TEM d (nm) | 3.4 | 4.7 | 2.4 |
| APT d (nm) | 1.7 | 5.8 | 2.5 |
| SANS d (nm) | 2.8 | 5.4 | 2.8* |
| TEM N ($10^{23}$ $m^{-3}$) | 1.2 | 0.6 | 2.8 |
| APT N ($10^{23}$ $m^{-3}$) | 2.9 | 0.7 | 9.6 |
| SANS N ($10^{23}$ $m^{-3}$) | 11 | 0.5 | 7.1* |
| SANS f (%) | 1.2 | 0.4 | 0.8 |
| APT Y/Ti/O | 23/37/41 | 22/31/46 | 11/42/47 |
| Microhardness ($kg/mm^2$) | 443±12 | 252±7 | 368±4 |

**Equivalent milled and annealed powder*

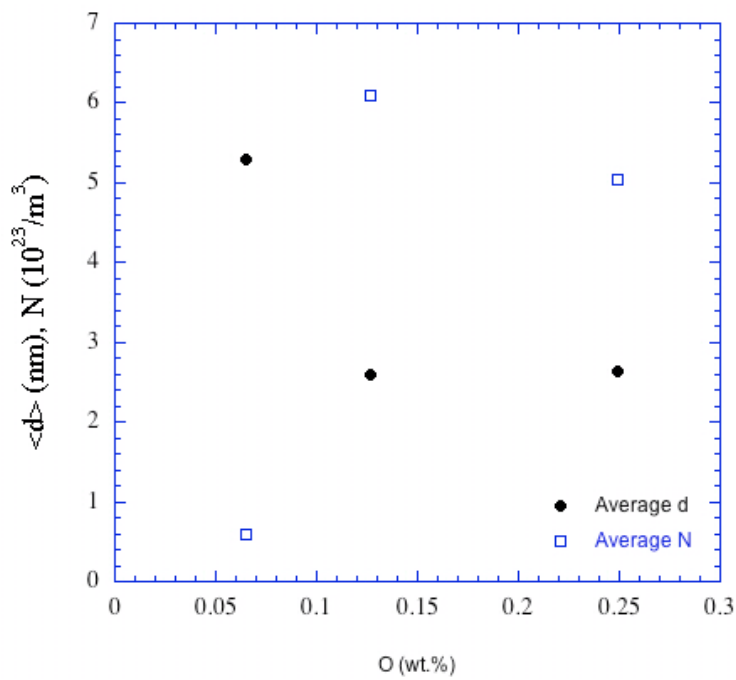


**Figure 7. The average of <d> and N for TEM, APT and SANS vs O content.**

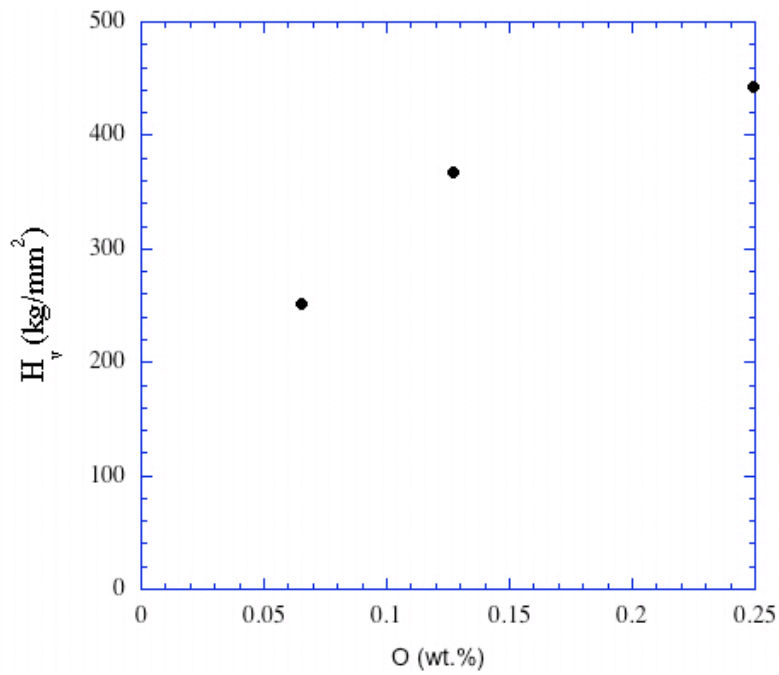


**Figure 8. The alloy $H_v$ versus O content.**

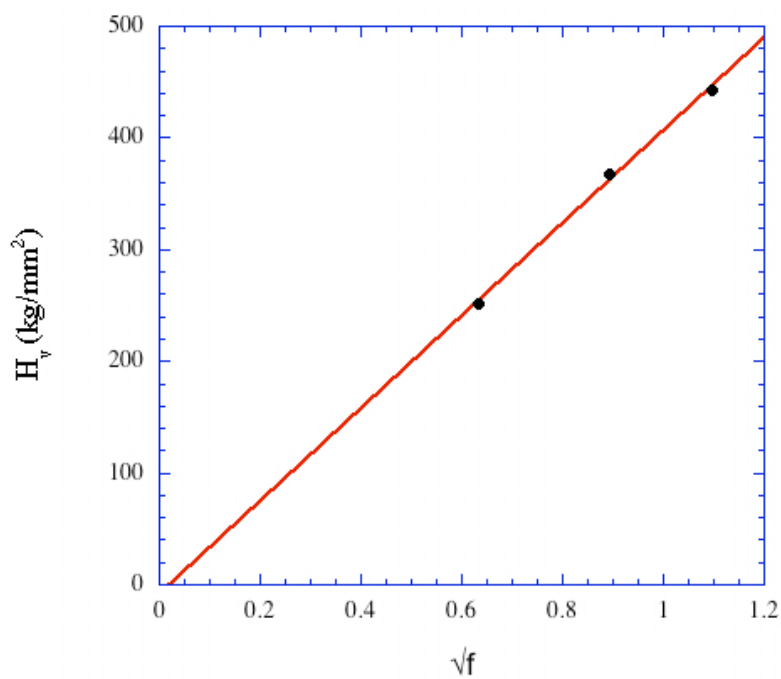


**Figure 9. The alloy $H_v$ versus the square root of the NF volume fraction ($\sqrt{f}$) measured by SANS.**

## FUTURE WORK

A journal paper will be prepared describing these results and submitted for publication.

## ACKNOWLEDGEMENT

This work was carried out as part of a multi-laboratory collaboration, led by S. Maloy (LANL) between LANL, UCSB and ORNL that was supported by the DOE Office of Nuclear Energy Fuel Cycle R&D Program. The research at UCSB and UC Berkeley was supported by subcontracts from LANL as well as a NERI grant at UCSB. A smaller contribution to this research was also made by the DOE Office of Fusion Energy.

## REFERENCES

1. S. Ohtsuka, S. Ukai, M. Fujiwara, T. Kaito, T. Narita, *J. Nucl. Mater.* **329**, 372 (2004).
2. S. Ohtsuka, S. Ukai, M. Fujiwara, T. Kaito, T. Narita, *J. Phys. Chem. of Solids* **66**, 571 (2005).
3. S. Ukai, S. Ohtsuka, *Energy Materials* **2**, 26 (2007).
4. S. Maloy et al., "Final Report on Improved Processing and Fabrication of Advanced, adiation-tolerant ODS Steels," LANL report LA-UR-11-10289, 2/28/11.